Quantitative analysis of the proliferative-to-invasive transition of hypoxic glioma cells†

Hector Gomez*[a]

Hypoxia is a hallmark of gliomas that is often associated with poor prognosis and resistance to therapies. Insufficient oxygen supply reduces the proliferation rate of tumor cells, which contributes to a slower progression of the lesion, but also increases the invasiveness of the tumor, making it more aggressive. To understand how these two counteracting mechanisms combine and modify the tumor's global growth, this paper proposes a quantitative approach based on a biomathematical model. The model predicts that the net effect of the proliferative-to-invasive transition leads to a lower survival even for slight increments of the invasive capacity of hypoxic tumor cells. The model also shows that tumor cells use the phenotype change to normalize the levels of oxygen in the tissue. The model results can be directly compared to *in vivo* data obtained using anatomic and molecular imaging modalities.

1 Introduction

Primary brain tumors are a major health problem and constitute the leading cause of cancer-related deaths in people below age 19. Approximately 80% of malignant primary brain tumors are gliomas. Glioma is a generic term used to describe cancerous tumors that originate in glial cells. Gliomas are classified into different grades according to their malignancy. Grades I and II are referred to as low grades, whereas grades III and IV are high grades. Glioblastoma multiforme (GBM) is a high-grade glioma characterized by diffuse invasion and high-rate proliferation. In spite of receiving extensive treatment in the form of surgical resection, radiation and chemotherapy, GBM patients have a poor prognosis and usually succumb to cancer in 6-12 months. New methods for the diagnosis and treatment of GBM are sorely needed.

In the last few years, patient-specific mathematical modeling has established itself as a promising tool for personalized diagnosis and treatment of GBM. It may be argued that GBM is an ideal candidate for patient-specific mathematical modeling for two reasons: First, GBM is noted for behaving differently across patients, which suggests that the treatment and management of the disease should be personalized. Second, GBM patients are usually diagnosed and monitored with anatomic (e.g., magnetic resonance) and molecular (e.g., positron emission tomography) imaging modalities, which provides a plethora of data that can be integrated into mathematical models[1]. Mathematical modeling of GBM has led to significant advances in brain tumor research. For example, mathematical models permitted understanding the relation between image-estimated growth kinetics and prognosis[2], quantifying the role of angiogenesis[3], or explaining edema formation[4]. This paper proposes a computational model to evaluate quantitatively the proliferative-to-invasive transition than hypoxia induces in gliomas.

Hypoxia has been often observed in GBM[5]. Insufficient oxygen supply has been associated with lower median survival and resistance to therapies in brain tumors[6–8], but the reasons for this remain unclear. There is strong evidence indicating that hypoxia increases migration and invasion in glioblastoma[9]. In particular, GBM cells subjected to hypoxic conditions express high levels of mesenchymal transcription factors. The overexpression of these transcription factors is associated with poor prognosis[10]. Patients with a mesenchymal phenotype have been observed to have significant levels of necrosis[11] and host tumors with a greater invasive potential[11,12]. Studies with cell cultures are consistent with these observations. In particular, the exposure of U87, SNB75 and U251 cells to hypoxia produced a cellular morphology markedly different to that of cells cultured in normoxic conditions. The cells under hypoxic conditions had a more elongated shape and were more loosely arranged than cells cultured in normoxic conditions[9]. This evidence has been often used to explain why hypoxia is associated with poor prognosis. However, it is also well known that glioblastoma cells display reduced proliferation under hypoxic conditions[13], which could also lead to a slower tumor progression. The fact that we have two counteracting mechanisms suggests that a quantitative approach could be useful.

This paper extends the classical proliferation-invasion mathematical model to account for the proliferative-to-migratory phenotype change in the presence of hypoxia. This is accomplished by introducing an equation that governs the oxygen dynamics and making the proliferation rate and the migration capacity of the tumor cells depend on oxygen concentration. The theory allows to

*email: hectorgomez@purdue.edu

[a] *School of Mechanical Engineering, Purdue University, 585 Purdue Mall, West Lafayette, IN, USA.*

study the impact of this phenotype change in the global tumor growth kinetics. The model predicts that for realistic values of the proliferation rate under hypoxic conditions, even mild increments of the invasive potential of the tumor cells lead to poorer prognosis and lower survival.

The model results can be directly compared to *in vivo* information obtained from medical images. In particular, the tumor cell density can be estimated from T2-weighted magnetic resonance images (MRIs) and the oxygen concentration from the ^{18}F-FMISO-PET imaging modality. The methodology could be used in conjunction with other computational approaches that focus on the impact of hypoxia on the tumor's resistance to therapy[14,15].

2 Materials and methods

Our methodology is based on a biomathematical model that accounts for tumor and oxygen dynamics. This section presents the model equations, an estimate of the model parameters and our computational method.

2.1 Biomathematical model

Our biomathematical model is based on the proliferation-invasion framework proposed by Murray and Alvord[16] and further studied by Swanson and coworkers[3,4,17]; see also[18–22]. The model assumes that the rate of change of tumor cell density is given by the net migration of tumor cells plus the proliferation of cancerous cells, namely

$$\frac{\partial c}{\partial t} = \nabla \cdot (D(\boldsymbol{x},\sigma)\nabla c) + \rho(\sigma)c\left(1-\frac{c}{k}\right). \tag{1}$$

Here, c is the tumor cell density, σ is the oxygen concentration, D is the diffusion coefficient of tumor cells that accounts for migration and ρ is the proliferation rate. The term $\rho(\sigma)c\left(1-\frac{c}{k}\right)$ in Eq. (1) represents the so-called logistic growth, which assumes that tumor cells proliferate until they reach the cell density k. The constant k is known as carrying capacity and represents the maximum number of tumor cells that can fit in 1 mm^3 of tissue. The novelty of our model is that we allow D and ρ to depend on the oxygen concentration σ. This allows us to account for the proliferative-to-migratory phenotype change promoted by hypoxia. We assume that ρ and D depend linearly on the oxygen concentration. In particular, we take

$$\rho(\sigma) = \rho_{max}\left[\frac{\sigma}{\sigma^v} + \alpha\left(1-\frac{\sigma}{\sigma^v}\right)\right] \tag{2}$$

$$D(\boldsymbol{x},\sigma) = D_{min}(\boldsymbol{x})\left[\frac{\sigma}{\sigma^v} + \beta\left(1-\frac{\sigma}{\sigma^v}\right)\right] \tag{3}$$

where ρ_{max}, α and β are constant parameters. ρ_{max} and $D_{min}(\boldsymbol{x})$ are, respectively, the proliferation rate and diffusion coefficient of tumor cells under normoxic conditions. D_{min} depends on the spatial coordinate $\boldsymbol{x}$ because tumor cells invade white matter faster than grey matter. The constant σ^v represents the oxygen concentration in blood vessels, which can be measured *in vivo* in a patient-specific manner.

To close the model we need another equation governing oxygen dynamics. This is usually modeled using reaction-diffusion equations. The reaction terms account for the oxygen consumed by cells and the amount that enters the tissue from blood vessels[23–25]. We use the equation

$$\frac{\partial \sigma}{\partial t} = D_{ox}\Delta\sigma - \frac{A_{ox}\sigma}{k_{ox}+\sigma}\frac{c}{k} + P_{er}S_v(\sigma^v - \sigma) \tag{4}$$

where D_{ox} is the diffusion constant of oxygen, A_{ox} and k_{ox} are the oxygen uptake parameters, P_{er} is the vascular permeability that modulates the release of oxygen across vessel walls and S_v is the vascular density, which is assumed to be constant. The first term of the right-hand side accounts for the isotropic diffusion of oxygen, the second for the oxygen uptaken by tumor cells, assuming Michaelis-Menten kinetics, and the third one considers that oxygen is released from blood vessels at a linear rate.

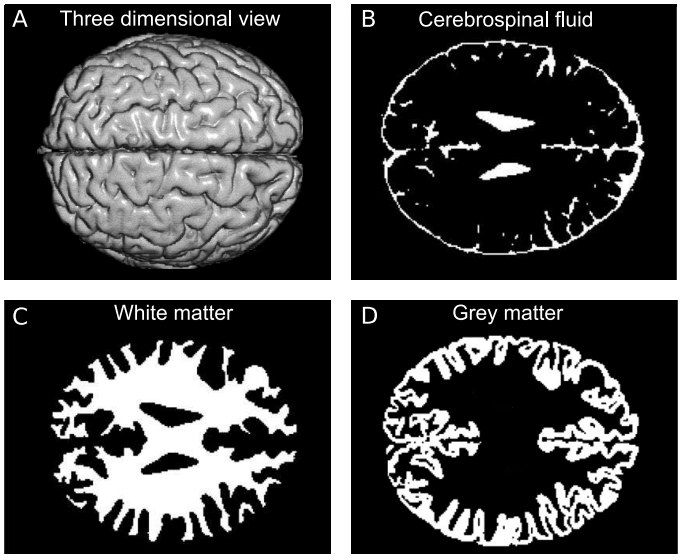

Fig. 1 We use the Brainweb phantom to obtain the geometry and the tissue distribution in the brain. The phantom provides a three-dimensional geometry of the brain (A) and a partition of the brain into several tissue types. Panels B, C and D show, respectively, the cerebrospinal fluid, white matter and black matter in a two-dimensional slice of the brain.

2.2 Anatomic model

The growth of tumor cells depends strongly on the anatomy of the brain, which defines the computational domain where the model equations are satisfied. The Brainweb phantom[26] was used to define the brain's anatomy. The phantom provides a voxel-wise map that describes the three-dimensional geometry of the brain; see Fig. 1A. It also provides a partition of the brain into white matter, grey matter and cerebrospinal fluid; see Figs. 1B-D where we show the different tissue types for a slice of the brain. This subdivision of the tissue is useful because D_{min} is smaller in grey matter than in white matter. We incorporated this observation in the model by taking

$$D_{min}(\boldsymbol{x}) = \begin{cases} D_w, & \boldsymbol{x} \in \text{ white matter}, \\ D_g, & \boldsymbol{x} \in \text{ grey matter}. \end{cases} \tag{5}$$

A usual assumption is that $5 \leq D_w/D_g \leq 50$; see, e.g., the work of Swanson et al.[27].

Table 1 Model parameters

Parameter	Value	Source
D_w	12.84 mm^2 year^{-1}	Ref.[4]
D_g	2.57 mm^2 year^{-1}	Ref.[4]
ρ_{max}	13.82 year^{-1}	Ref.[4]
k	2×10^6 cells mm^{-3}	Ref.[4]
D_{ox}	56575 mm^2 year^{-1}	Ref.[25]
A_{ox}	4.03×10^{-4} mol year^{-1} mm^{-2}	Ref.[28]
k_{ox}	5×10^{-12} mol mm^{-3}	Ref.[28]
P_{er}	11.31×10^6 mm year^{-1}	Ref.[25]
S_v	10 mm^{-1}	Ref.[25]
σ^v	2×10^{-10} mol mm^{-3}	Ref.[25]

2.3 Parameter estimation

All the model parameters can be obtained directly from the literature (see Table 1), except α and β in Eqs. (2) and (3). The impact of oxygen concentration into the proliferative and invasive capacity of GBM is usually disregarded in mathematical models, which makes it difficult to find estimates of α and β in the literature. This paper proposes a procedure to estimate α from data of GBM spheroids[13]. These data provide the time evolution of the cell density for different values of oxygen concentration. The experimental data is taken from[13] and represented in Fig. 2 with squares and circles. The plot shows tumor cell density for normoxic (8% O_2; squares) and hypoxic (1% O_2; circles) conditions.

The model can be applied to this situation by assuming σ to be constant, as in the experiment, and manipulating Eq. (1). We note that $0 \le c(\boldsymbol{x},t) \le C(t)$, where $C(t)$ is an upper bound for the tumor cell density that satisfies the ordinary differential equation

$$\frac{\mathrm{d}C}{\mathrm{d}t} = \rho C(1-C/k). \tag{6}$$

The solution to Eq. (6) with the initial condition $C(0) = C_0$ is

$$C(t) = \frac{C_0 k \exp(\rho(\sigma)t)}{k + C_0(\exp(\rho(\sigma)t) - 1)} \tag{7}$$

where k is taken from Table 1. Taking C_0 and $C(t)$ from the experimental data in Fig. 2, we can estimate ρ for different values of σ using the relation

$$\rho(\sigma) = \frac{1}{t}\log\left(\frac{C(t)(C_0-k)}{C_0(C(t)-k)}\right) \tag{8}$$

which follows directly from (7). By using Eq. (8) for the two values of oxygen concentration in Fig. 2, we estimate $\alpha \approx 0.6$.

We have been unable to estimate the parameter β using data from the literature. We have selected a set of values for β and performed most of our simulations using all those values. This allows to understand the dependence of the solution on β.

2.4 Computational method

Computing a numerical solution of Eqs. (1)–(4) on the brain geometry poses significant challenges for conventional numerical methodologies due to the nonlinearity of the equations, the complicated geometry of the brain and the disparity of time scales of Eq. (1) and Eq. (4). The latter is a consequence of tumor dynamics being much slower than oxygen dynamics.

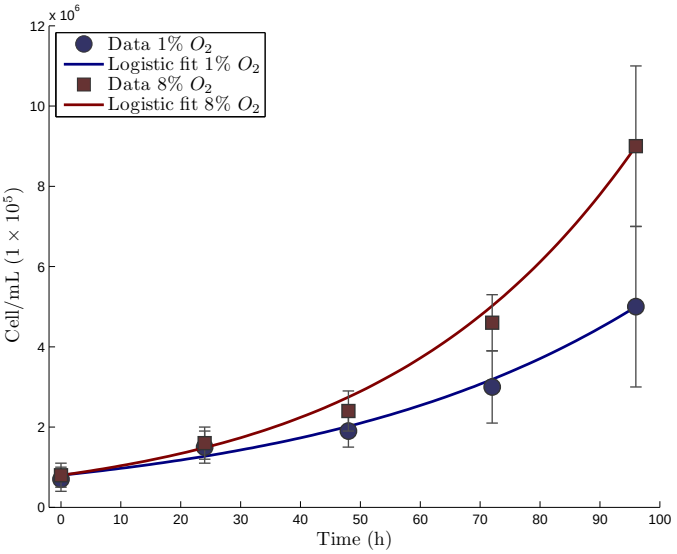

Fig. 2 Time evolution of the tumor cell density in GBM spheroids. Experimental data in normoxic (8% O_2; squares) and hypoxic (1% O_2; circles) conditions taken from[13]. The solid lines represent plots of Eq. (7) keeping k fixed and computing ρ from Eq. (8).

To avoid the complex process of generating a mesh that defines the brain geometry we resort to the so-called diffuse domain method[29]. This permits to embed the geometry of the brain on a larger cube that acts as computational domain. Then, we restrict the equations to the brain's geometry using a smooth field that can be obtained from a medical image or the Brainweb phantom[26]. Space discretization is performed using a pseudospectral collocation method[30]. The time integration scheme is a third-order accurate Runge-Kutta method.

For simplicity, the numerical simulations presented in this paper are performed on a two-dimensional slice of the brain. The extension to three dimensions is straightforward, although computationally intensive.

3 Results

3.1 The model reproduces key features of GBM

Fig. 3 shows the time evolution of the tumor cell density (top row) and oxygen concentration (bottom row) using $\alpha = 0.6$ and $\beta = 10$. The plot shows how the tumor grows invasively producing hypoxia in the tissue. The hypoxic region grows radially leading to a traveling-wave pattern similar to that observed in ^{18}F-FMISO-PET images[31,32]. It was verified that this prediction of the model is robust with respect to the tumor location and size.

For comparison purposes, Fig. 4 shows an identical computation but taking $\alpha = \beta = 1$. In this case, the tumor growth equation becomes the classical Fisher-Kolmogorov model in which proliferation and invasion are insensitive to oxygen concentration; see Eqns. (2) and (3). The plot shows that in the absence of the phenotype change, the tumor is less invasive and easier to detect on magnetic resonances due to the higher cellular density.

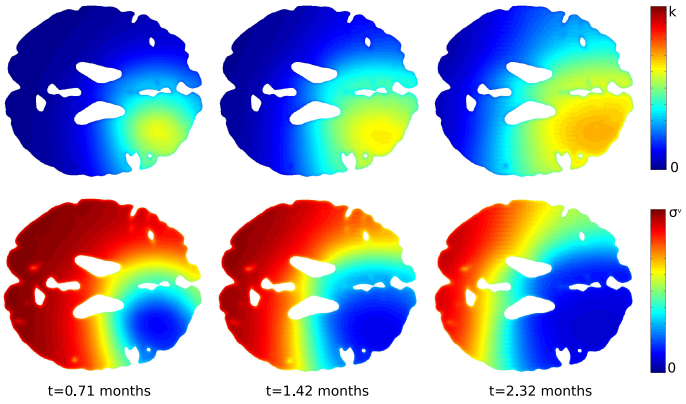

Fig. 3 Time evolution of tumor (top row) and oxygen concentration (bottom row) for $\alpha = 0.6$ and $\beta = 10$. The rest of the parameters are taken from Table 1. The plot shows how the tumor expands with time and the hypoxic region grows accordingly.

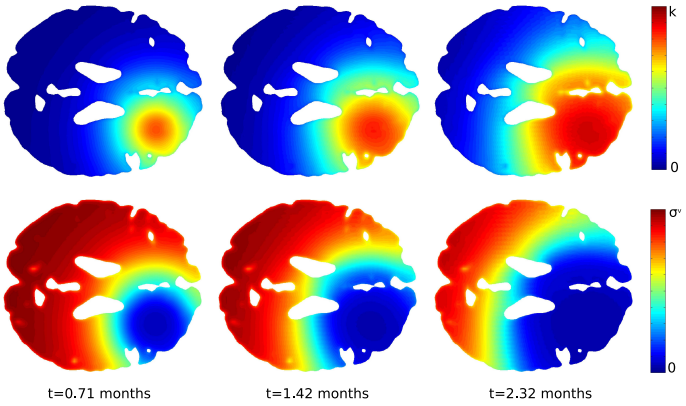

Fig. 4 Time evolution of tumor (top row) and oxygen concentration (bottom row) for $\alpha = \beta = 1$. In this case the tumor equation corresponds to the classical Fisher-Kolmogorov model, where ρ and D are independent from oxygen concentration. The rest of the parameters are taken from Table 1.

This can be better appreciated in Fig. 5A, which shows the time evolution of the maximum cellular density in the brain normalized with respect to the carrying capacity ($\max(c)/k$; red line) for the classical Fisher-Kolmogorov model ($\alpha = \beta = 1$; dashed line) and the proposed model ($\alpha = 0.6$, $\beta = 10$; solid line). The blue lines in Fig. 5A display the time evolution of $\min(\sigma)/\sigma^v$, where $\min(\sigma)$ denotes the minimum oxygen concentration in the brain. The dashed line represents the Fisher-Kolmogorov model and the solid line the case $\alpha = 0.6$, $\beta = 10$. Interestingly, the data suggest the the tumor uses the proliferative-to-invasive transition to escape hypoxia. As a consequence of the phenotype switch, the minimum value of σ is increased by approximately a factor of 2. An additional illustration of this phenomenon is presented in Fig. 5B, which shows that the area of the brain under acute hypoxia ($\sigma < \sigma^v/10$) is significantly larger when the phenotype change is not considered ($\alpha = \beta = 1$).

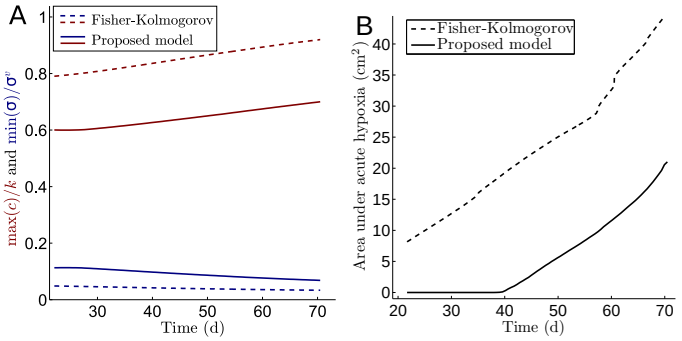

Fig. 5 A: Time evolution of the normalized maximum cell density (red lines) for the Fisher-Kolmogorov model (dashed line) and the proposed model (solid line). The blue lines show analogous data for the normalized minimum oxygen concentration. B: Time evolution of the area under acute hypoxia ($\sigma < \sigma^v/10$) for the Fisher-Kolmogorov model (dashed line) and the proposed model (solid line).

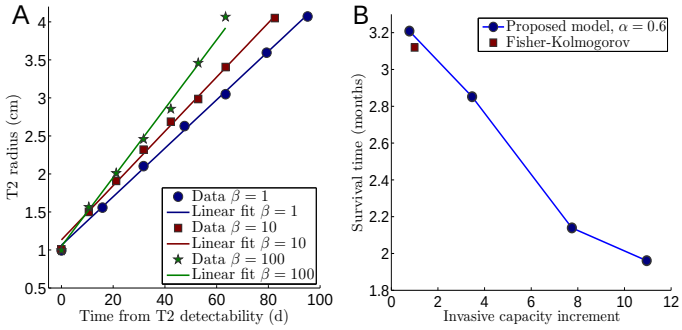

Fig. 6 A: Time evolution of the tumor's T2-radius for $\alpha = 0.6$. We use $\beta = 1$ (blue circles), $\beta = 10$ (red squares) and $\beta = 100$ (green stars). We also show linear approximations of the data (solid lines) to confirm that the T2-radius grows linearly. B: Survival time versus the invasive capacity increment. The red square represents a reference solution for the classical Fisher-Kolmogorov model ($\alpha = \beta = 1$), while the blue circles correspond to $\alpha = 0.6$ and several values of the invasive capacity increment.

3.2 Despite the phenotype change the tumor grows with constant imageable velocity

In spite of the significant heterogeneity of gliomas, the radius of the image-detectable part of the tumor has been shown to grow linearly. This was accomplished by Mandonnet et al.[33] who collected serial images of untreated patients with grade II gliomas. The classical Fisher-Kolmogorov model in which ρ and D are constants produces linear growth of the tumor radius with asymptotic velocity $2\sqrt{D\rho}$. This result does not necessarily hold true for the proposed model because D and ρ vary in space and time as a function of the oxygen concentration. To check the hypothesis of linear growth, we created a virtual tumor using an exponential initial condition for the field c. We assumed that the region of the tumor visible in a T2-weighted MRI is that in which $c > 4 \times 10^5$ cells/mm^3. We started the simulation using a tumor with a T2-radius of 1 cm. We let the simulation evolve until the T2-radius was 4 cm, which is usually assumed to lead to the patient's death. Fig. 6A shows that, in spite of the phenotype change, the T2 radius grows linearly for all tested values of β. We used $\alpha = 0.6$ in all cases.

3.3 The proliferative-to-invasive transition decreases survival

To study of the impact of the proliferation-to-migration transformation on the survival time, a reference simulation was performed taking $\alpha = \beta = 1$, which corresponds to the classical Fisher-Kolmogorov model. Then, we took the value $\alpha = 0.6$, which has been estimated from experiments, and repeated the simulation for several values of β. The results are plotted in terms of the invasive capacity increment $\sqrt{\alpha\beta}$. The quantity $\sqrt{\alpha\beta}$ is an estimate of v_{hyp}/v_{nor} where v_{hyp} (respectively, v_{nor}) is the invasive velocity of the tumor in hypoxic (respectively, normoxic) conditions. The estimate is based on the Fisher-Kolmogorov traveling wave solution. The reference solution ($\alpha = \beta = 1$) has been plotted with a red square in Fig. 6B. The blue circles represent the survival time for $\alpha = 0.6$ and different values of the invasive capacity increment. The survival time has been measured by placing in the brain a virtual tumor with a T2-radius of 1 cm and letting the simulation evolve until the T2-radius became 4 cm.

The plot shows that when the proliferative-to-invasive phenotype switch is accounted for, the survival time decreases even for very modest values of the invasive capacity increment.

4 Discussion

Hypoxia has been often observed in gliomas. Low oxygen concentration triggers a proliferative-to-invasive transition in brain tumor cells. This paper proposes a biomathematical model to quantitatively understand the impact of this transition on the global growth kinetics of the lesion. The model extends previous theoretical efforts by accounting for the dependence of the proliferation rate and the diffusion coefficient of tumor cells on oxygen concentration. Oxygen dynamics in the brain tissue is modeled using standard reaction-diffusion equations.

The model predicts that the proliferative-to-invasive transition leads to lower survival even for slight increments of the invasive capacity of hypoxic tumor cells. The model also suggests that the phenotype change contributes to restore normoxic conditions and is used by tumor cells as a self-control mechanism. The proposed biomathematical model can be used in combination with other computational methods that aim at studying the influence of hypoxia on the effectiveness of radiation therapy[14]. The proposed methodology could also be used to study how hypoxia acts differently across glioma grades[34].

Although we illustrated the concept theoretically, the model has significant potential to incorporate *in vivo* patient-specific data. The cellular density can be estimated using T2-weighted MRIs or, even better, diffusion weighted images. The proliferation rate and the diffusion coefficient of tumor cells can also be estimated on a patient-specific basis using serial images[1]. The oxygen concentration can be estimated using ^{18}F-FMISO-PET images. The parameters of the oxygen dynamics equation could also be inferred from serial molecular images.

The major limitation of the model is that we have been unable to estimate the parameter β using data from the literature. Although the main conclusions of the paper are almost insensitive to β, it would be very interesting to design an experiment to estimate β. Another restriction of the study is that the simulations have been performed on two-dimensional slices of the brain. Although this is unlikely to have an impact on the main conclusions of the paper, future research should be devoted to perform fully three-dimensional patient-specific simulations.

Acknowledgments

HG was partially supported by the European Research Council through the FP7 Ideas Starting Grant Program (Contract #307201) and by Xunta de Galicia, co-financed with FEDER funds.

References

1 T. E. Yankeelov, N. Atuegwu, D. Hormuth, J. A. Weis, S. L. Barnes, M. I. Miga, E. C. Rericha and V. Quaranta, *Science translational medicine*, 2013, **5**, 187ps9–187ps9.

2 C. H. Wang, J. K. Rockhill, M. Mrugala, D. L. Peacock, A. Lai, K. Jusenius, J. M. Wardlaw, T. Cloughesy, A. M. Spence, R. Rockne *et al.*, *Cancer research*, 2009, **69**, 9133–9140.

3 K. R. Swanson, R. C. Rockne, J. Claridge, M. A. Chaplain, E. C. Alvord and A. R. Anderson, *Cancer research*, 2011, **71**, 7366–7375.

4 A. Hawkins-Daarud, R. C. Rockne, A. R. Anderson and K. R. Swanson, *Frontiers in oncology*, 2013, **3**, 66.

5 S. M. Evans, K. D. Judy, I. Dunphy, W. T. Jenkins, W.-T. Hwang, P. T. Nelson, R. A. Lustig, K. Jenkins, D. P. Magarelli, S. M. Hahn, R. A. Collins, M. S. Grady and C. J. Koch, *American Association for Cancer Research*, 2004, **10**, 8177–8184.

6 C.-H. Hsieh, W.-C. Shyu, C.-Y. Chiang, J.-W. Kuo, W.-C. Shen and R.-S. Liu, *PloS one*, 2011, **6**, e23945.

7 B. Liang, *Journal of Neuro-Oncology*, 1996, **29**, 149–155.

8 S. Sathornsumetee, Y. Cao, J. E. Marcello, J. E. Herndon, R. E. McLendon, A. Desjardins, H. S. Friedman, M. W. Dewhirst,

J. J. Vredenburgh and J. N. Rich, *Journal of Clinical Oncology*, 2008, **26**, 271–278.

9 J. V. Joseph, S. Conroy, K. Pavlov, P. Sontakke, T. Tomar, E. Eggens-Meijer, V. Balasubramaniyan, M. Wagemakers, W. F. den Dunnen and F. A. Kruyt, *Cancer letters*, 2015, **359**, 107–116.

10 L. A. Cooper, D. A. Gutman, C. Chisolm, C. Appin, J. Kong, Y. Rong, T. Kurc, E. G. V. Meir, J. H. Saltz, C. S. Moreno and D. J. Brat, *The American Journal of Pathology*, 2012, **180**, 2108 – 2119.

11 R. G. Verhaak, K. A. Hoadley, E. Purdom, V. Wang, Y. Qi, M. D. Wilkerson, C. R. Miller, L. Ding, T. Golub, J. P. Mesirov, G. Alexe, M. Lawrence, M. O'Kelly, P. Tamayo, B. A. Weir, S. Gabriel, W. Winckler, S. Gupta, L. Jakkula, H. S. Feiler, J. G. Hodgson, C. D. James, J. N. Sarkaria, C. Brennan, A. Kahn, P. T. Spellman, R. K. Wilson, T. P. Speed, J. W. Gray, M. Meyerson, G. Getz, C. M. Perou and D. N. Hayes, *Cancer Cell*, 2010, **17**, 98 – 110.

12 M. S. Carro, W. K. Lim, M. J. Alvarez, R. J. Bollo, X. Zhao, E. Y. Snyder, E. P. Sulman, S. L. Anne, F. Doetsch, H. Colman *et al.*, *Nature*, 2010, **463**, 318–325.

13 R. Richards, M. D. Jenkinson, B. J. Haylock and V. See, *PeerJ*, 2016, **4**, e1755.

14 R. C. Rockne, A. D. Trister, J. Jacobs, A. J. Hawkins-Daarud, M. L. Neal, K. Hendrickson, M. M. Mrugala, J. K. Rockhill, P. Kinahan, K. A. Krohn *et al.*, *Journal of the Royal Society Interface*, 2015, **12**, 20141174.

15 A. M. Spence, M. Muzi, K. R. Swanson, F. O'Sullivan, J. K. Rockhill, J. G. Rajendran, T. C. Adamsen, J. M. Link, P. E. Swanson, K. J. Yagle *et al.*, *Clinical Cancer Research*, 2008, **14**, 2623–2630.

16 G. C. Cruywagen, D. E. Woodward, P. Tracqui, G. T. Bartoo, J. Murray and E. C. Alvord, *Journal of Biological Systems*, 1995, **3**, 937–945.

17 A. Baldock, R. Rockne, A. Boone, M. Neal, C. Bridge, L. Guyman, M. Mrugala, J. Rockhill, K. R. Swanson, A. D. Trister *et al.*, *Frontiers in oncology*, 2013, **3**, 62.

18 A. Martínez-González, G. F. Calvo, L. A. P. Romasanta and V. M. Pérez-García, *Bulletin of mathematical biology*, 2012, **74**, 2875–2896.

19 L. Pérez Romasanta, J. Belmonte Beitia, A. Martínez González, G. Fernández Calvo and V. Pérez García, *Reports of Practical Oncology & Radiotherapy*, 2013, **18**, S63.

20 V. M. Pérez-García, M. Bogdanska, A. Martínez-González, J. Belmonte-Beitia, P. Schucht and L. A. Pérez-Romasanta, *Mathematical Medicine and Biology*, 2014, 307–329.

21 A. Martínez-González, M. Durán-Prado, G. F. Calvo, F. J. Alcaín, L. A. Pérez-Romasanta and V. M. Pérez-García, *Mathematical Medicine and Biology*, 2014, dqu002.

22 O. Clatz, M. Sermesant, P.-Y. Bondiau, H. Delingette, S. K. Warfield, G. Malandain and N. Ayache, *IEEE transactions on medical imaging*, 2005, **24**, 1334–1346.

23 T. Roose, P. A. Netti, L. L. Munn, Y. Boucher and R. K. Jain, *Microvascular research*, 2003, **66**, 204–212.

24 Y. Kim, M. A. Stolarska and H. G. Othmer, *Progress in biophysics and molecular biology*, 2011, **106**, 353–379.

25 F. Mpekris, S. Angeli, A. P. Pirentis and T. Stylianopoulos, *Biomechanics and modeling in mechanobiology*, 2015, **14**, 1391–1402.

26 *Brainweb: simulated brain database*, http://brainweb.bic.mni.mcgill.ca/, Accessed: 2016-09-28.

27 K. R. Swanson, E. Alvord and J. Murray, *Cell proliferation*, 2000, **33**, 317–329.

28 J. J. Casciari, S. V. Sotirchos and R. M. Sutherland, *Journal of cellular physiology*, 1992, **151**, 386–394.

29 X. Li, J. Lowengrub, A. Rätz and A. Voigt, *Communications in mathematical sciences*, 2009, **7**, 81.

30 L. N. Trefethen, *Spectral methods in MATLAB*, Siam, 2000, vol. 10.

31 S. Gu, G. Chakraborty, K. Champley, A. M. Alessio, J. Claridge, R. Rockne, M. Muzi, K. A. Krohn, A. M. Spence, E. C. Alvord *et al.*, *Mathematical Medicine and Biology*, 2012, **29**, 31–48.

32 K. R. Swanson, G. Chakraborty, C. H. Wang, R. Rockne, H. L. Harpold, M. Muzi, T. C. Adamsen, K. A. Krohn and A. M. Spence, *Journal of Nuclear Medicine*, 2009, **50**, 36–44.

33 E. Mandonnet, J.-Y. Delattre, M.-L. Tanguy, K. R. Swanson, A. F. Carpentier, H. Duffau, P. Cornu, R. Van Effenterre, E. C. Alvord and L. Capelle, *Annals of neurology*, 2003, **53**, 524–528.

34 B. E. Lally, S. Rockwell, D. B. Fischer, D. R. Collingridge, J. M. Piepmeier and J. P. Knisely, *The Cancer Journal*, 2006, **12**, 461–466.